

## Production Yields of Neutron-Rich Fluorine Isotopes

E. Kwan<sup>1,2</sup>, D.J. Morrissey<sup>1,3</sup>, D.A. Davies<sup>1,3</sup>, M. Steiner<sup>1</sup>, C.S. Sumithrarachchi<sup>1,3</sup> and L. Weissman<sup>1</sup>

<sup>1</sup>National Superconducting Cyclotron Laboratory, Michigan State University, East Lansing, MI 48824, USA

<sup>2</sup>Department of Physics and Astronomy, Michigan State University, East Lansing, MI 48824, USA

<sup>3</sup>Department of Chemistry, Michigan State University, East Lansing, MI 48824, USA

*Received 31 October 2005*

**Abstract.** Two experiments were performed at the NSCL to investigate the momentum distributions from projectile fragmentation. An  $^{40}\text{Ar}$  beam reacted with three N/Z targets in order to determine the effects of the N/Z of the target on the production yields of neutron-rich fluorine isotopes. A  $^{48}\text{Ca}$  beam was then used with a Ta target to re-measure the production cross-sections and to determine the neutron drip-line of fluorine. The cross-sections are compared to the predictions from a deep inelastic transfer model and a semi-empirical model, EPAX 2.15.

*Keywords:* neutron drip-line, fluorine isotopes, projectile fragmentation, cross-sections

*PACS:* 25.70.Mn, 27.30.+t

### 1. Introduction

The determination of the locations of the drip-lines is of great importance in the understanding of how shell structure changes as nuclei become more exotic. The neutron drip-line has only been mapped up to oxygen with the non-observations of  $^{26}\text{O}$  and  $^{28}\text{O}$  [1–3]. It is unclear whether the neutron drip-line of fluorine has been reached. Table 1 contains the predicted one- and two-neutron separation energies for  $^{31,32,33}\text{F}$  from a Hartree-Fock (HF) model by Brown [4] and the Finite Range Droplet Model (FRDM) by Möller *et al* [5]. Both of these models predict  $^{31}\text{F}$  to be the last bound fluorine isotope, since  $^{33}\text{F}$  is predicted to be unbound against two-

At low energies, the exchange of nucleons during the interaction time between the target and projectile and/or the re-absorption of participant nucleons cause large neutron-to-proton ratio (N/Z) targets to influence the N/Z ratio of the observed fragments [6]. Two experiments were performed at the NSCL to investigate the production of the most neutron-rich nuclei by projectile fragmentation. The first experiment was performed to determine the effect of the target on the production yields at the intermediate energy of 140 MeV/nucleon. The results from the first experiment determined which reaction target to use to fragment the  $^{48}\text{Ca}$  beam. This second experiment re-measured the production yields and confirmed the location of the neutron drip-line of the oxygen-fluorine region.

**Table 1.** Predicted one- and two-neutron separation energies given in MeV from a HF model by Brown [4] and a FRDM model by Möller *et al.* [5].

Nuclei	$1S_n(\text{HF})$	$2S_n(\text{HF})$	$1S_n(\text{FRDM})$	$2S_n(\text{FRDM})$
$^{31}\text{F}$	1.95(12)	0.78(12)	3.84	2.46
$^{32}\text{F}$	-2.2(16)	0.1 (23)	-1.76	2.08
$^{33}\text{F}$	0.75(12)	-1.52(20)	-0.57	-2.32

## 2. Experimental Setup

An  $^{40}\text{Ar}^{18+}$  beam was accelerated through the coupled cyclotrons at  $\sim 49.5$  pA at the NSCL and allowed to react with either a  $658\text{ mg/cm}^2$  Be, a  $767\text{ mg/cm}^2$  Ni, or a  $1041\text{ mg/cm}^2$  Ta target. A second experiment used a  $^{48}\text{Ca}^{19+}$  beam also accelerated to  $140\text{ MeV/nucleon}$  at  $\sim 8.5$  pA and fragmented in a  $1181\text{ mg/cm}^2$  Ta target. The target thicknesses for both experiments were chosen to maximize the production of

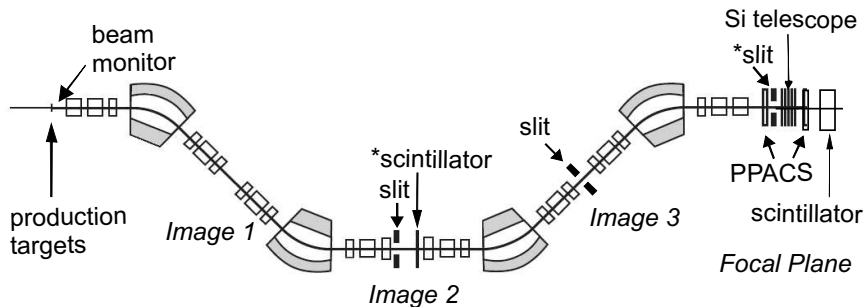


**Fig. 1.** Schematics of the A1900 Fragment Separator. \*Additions made to the configuration for the experiment with  $^{48}\text{Ca}+^{181}\text{Ta}$ .

$^{31}\text{F}$  and to give similar energy losses of the fragments of interest. A  $\text{BaF}_2$  detector located near the reaction targets was used to monitor the beam intensities, see Fig. 1. Fragments were selected and transmitted through the A1900 [7] using a 1% momentum acceptance. The rigidities ( $B\rho$ ) were set to the LISE [8] predicted maximum production peak of each fluorine isotope starting from  $^{22}\text{F}$  and  $^{25}\text{F}$  for the first and second experiments, respectively. At the largest rigidities, the A1900 was opened to the maximum momentum acceptance of 5% to observe the production of  $^{31}\text{F}$  and heavier fluorine isotopes. A  $30 \text{ mg/cm}^2$  BC-400 scintillator located at Image 2 was used to track the ions and to correct for deviations from the central trajectory. Five one-mm thick Si PIN detectors with an active area of  $50 \times 50 \text{ cm}^2$  and a 10-cm thick plastic scintillator located at the Focal Plane were used to measure the energy loss and total energy of the transmitted particles. The second Si detector and the scintillator also provided separate start signals for the radio frequency time-of-flight (TOF) measurements. Information from these detectors allowed all of the transmitted particles to be identified using a TOF technique.

### 3. Results

The momentum distributions in the lab frame for the six heaviest observed fluorine isotopes from the reaction of  $^{40}\text{Ar}$  on  $^9\text{Be}$ ,  $^{nat}\text{Ni}$  and  $^{181}\text{Ta}$  are shown in Fig. 2 depicted by the diamonds, squares and open circles, respectively. The convolution

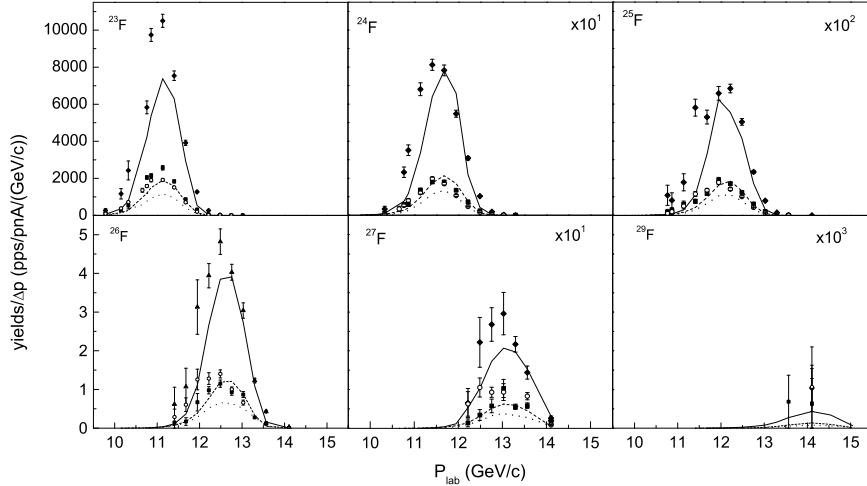


**Fig. 2.** Production yields from the reaction of  $^{40}\text{Ar}$  on  $^9\text{Be}$ ,  $^{nat}\text{Ni}$ , and  $^{181}\text{Ta}$  for the six heaviest observed fluorine isotopes shown by the diamonds, squares and open circles, respectively. The EPAX predicted values are shown by the solid, dashed and dotted curves for the Be, Ni and Ta targets, respectively.

model in the simulation program LISE under-predicts the width and heights of the momentum distributions from the Be and Ta targets (solid and dotted curves, respectively) while reproducing the yields from the Ni target (dashed curves) and the location of the centroids. The influence of the  $N/Z$  of the targets can be seen on the production yields of the fluorine isotopes, which is not reproduced by the theoretical calculations. At the peak of production, the Be target produces a factor of five times more  $^{23}\text{F}$  than the Ni and Ta targets. This factor decreases for more neutron-rich isotopes, so that at  $^{29}\text{F}$ , there is no difference in the yields from each target.

The cross-sections from both experiments were determined by fitting the yields with an asymmetric Gaussian function. At relativistic energies, the momentum distributions are expected to be Gaussian. However, at lower energies a low energy tail has been observed due to nucleon pick-up and dissipative processes [9]. The angular transmission of the fragments through the A1900 were calculated by LISE. Fig. 3 shows the cross-sections as a function of mass number from both experiments. The data from the reaction of  $^{40}\text{Ar}+^{nat}\text{Ni}$  (squares),  $^{40}\text{Ar}+^{181}\text{Ta}$  (circles), and  $^{48}\text{Ca}+^{181}\text{Ta}$  (stars) are offset by  $\pm 0.2$  mass units from the  $^{40}\text{Ar}+^9\text{Be}$  data (diamonds) for clarity. The cross-sections from the reaction of  $^{40}\text{Ar}+^{181}\text{Ta}$  is six and four times larger than the cross-sections from the Be and Ni targets, respectively for the most neutron-rich isotopes. The similar yields of  $^{29}\text{F}$  and the larger cross-sections of the Ta target relative to the other targets suggested that a Ta target should be used with the  $^{48}\text{Ca}$  to produce fluorine isotopes heavier than  $^{29}\text{F}$ . The effect of the  $N/Z$  of the projectile can also be seen in the data. A factor of three increase can be seen in the cross-sections for the most exotic fluorine isotopes from the

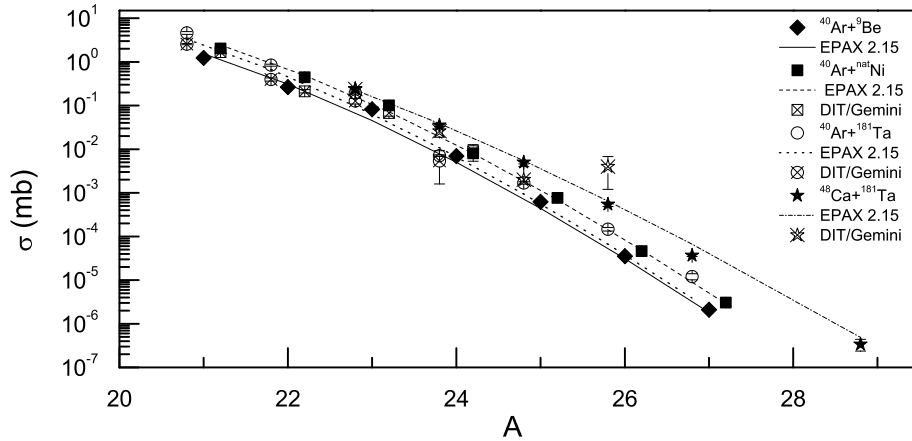


**Fig. 3.** The measured and theoretical cross-sections predicted by DIT/GEMINI and EPAX 2.15. Data from the reaction of  $^{40}\text{Ar}$  with the  $^{nat}\text{Ni}$  and  $^{181}\text{Ta}$  targets and  $^{48}\text{Ca}+^{181}\text{Ta}$  are offset by  $\pm 0.2$  A for clarity.

experiment with  $^{48}\text{Ca}$  compared to the  $^{40}\text{Ar}+^{181}\text{Ta}$  experiment. The cross-sections calculated from EPAX [12] and a deep inelastic transfer (DIT) [13] code coupled to a de-excitation code GEMINI [14], shown by the curves and the crossed data points, respectively, are able reproduce the measured cross-sections, the solid and unfilled points, to within a factor of three, with the exception of  $^{26}\text{F}$ . The cross-sections from the DIT model were only calculated up to  $^{24}\text{F}$  and  $^{26}\text{F}$  for the first and second experiment, respectively, due to the statistical nature of the code. Due to the size of the Be target, the DIT code was unable to calculate the cross-sections. The reproduction of the cross-sections from the DIT code for the heavy targets suggests that deep inelastic transfers known to occur at low energies near the Fermi energy can still persist at 140 MeV/nucleon.

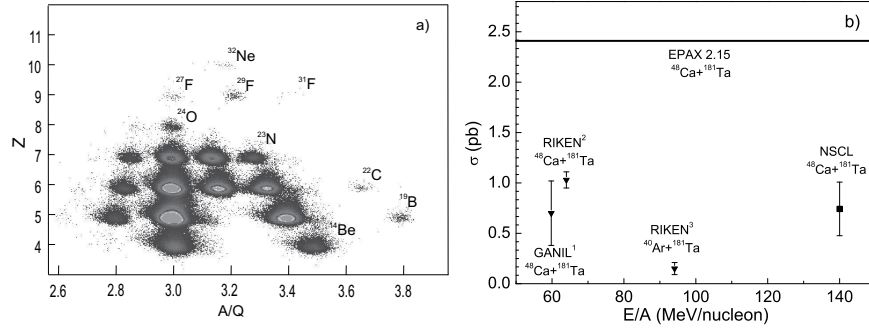


**Fig. 4.** a) Particle identification of  $^{31}\text{F}$  produced from the reaction of  $^{48}\text{Ca}+^{181}\text{Ta}$ . b) The cross-sections of  $^{31}\text{F}$  as a function of projectile energy. <sup>1,2,3</sup> Data from references [10], [11] and [2], respectively. The data point (square) at the highest incident energy is from the present work. The horizontal line is the predicted cross-section by EPAX for  $^{48}\text{Ca}$  on  $^{181}\text{Ta}$ .

Fig. 4a shows the combined Z vs A/Q plot calculated with the average energy loss and the TOF from the A1900 tunes optimized for  $^{31}\text{F}$  and  $^{32}\text{F}$ . Eight  $^{31}\text{F}$  ions were observed over a two day period. Five particles were observed at  $B\rho$  settings of 5.5139/5.5016 Tm for the first and second half of the A1900, respectively, and three particles were observed at  $B\rho=5.7154/5.7032$  Tm. There were no observations of  $^{26}\text{O}$ ,  $^{28}\text{O}$ ,  $^{28}\text{F}$  and  $^{30}\text{F}$ . The systematic variation of the centroids and widths of the Gaussian momentum distributions were measured to predict the shape of the Gaussian of  $^{31}\text{F}$ . Fig. 4b shows the cross-section from the reaction of  $^{48}\text{Ca}+^{181}\text{Ta}$  obtained from this work (square) compared to other published results from RIKEN and GANIL (triangles) and EPAX (horizontal line) as a function of projectile energy. Statistical errors were assumed for the cross-section from ref. [10]. EPAX is unable to reproduce the measured cross-sections and over-predicts the cross-sections by a

factor of two, while the experimental results from RIKEN, GANIL, and MSU show no dependence of the cross-section on the incident energy. No further attempt was made to explore for the existence of  $^{33}\text{F}$ , which would require an additional four months to produce one count under the present experimental conditions.

## 4. Conclusion

We found that the  $N/Z$  of the target influences the production yields of the heavy fluorine isotopes. The exchange of nucleons during the interaction between the projectile and target can explain the reaction process at an intermediate energy of 140 MeV/nucleon to produce neutron-rich fragments. The similar production yields of  $^{29}\text{F}$  from all three reaction targets in the first experiment and the cross-sections for the heaviest isotopes suggested that the Ta target should be used in the second experiment to explore the fluorine drip-line. There were no observation of  $^{28}\text{F}$  or  $^{30}\text{F}$ . The existence of  $^{31}\text{F}$  has been confirmed with a measured cross-section of 0.74(27) pb from the reaction of  $^{48}\text{Ca}$  on  $^{181}\text{Ta}$ . This result is in agreement with other literature values.

## Acknowledgments

The authors would like to thank G.A. Souliotis for his assistance with the DIT/Gemini calculations. This work was supported by the National Science Foundation under the grant No. PHY-01-01523.

## References

1. M. Thoennessen, *Rep. Prog. Phys.* **67** (2004) 1187.
2. H. Sakura *et al.*, *Phys. Lett. B* **448** (1999) 180.
3. M. Fauerbach *et al.*, *Phys. Rev. C* **53** (1996) 647.
4. B.A. Brown, *Prog. Part. Nucl. Phys.* **47** (2001) 517.
5. P. Möller *et al.*, *At. Data and Nucl. Data Tables* **66** (1997).
6. D. Guerreau, *Nucl. Phys.* **A447** (1985) 37c.
7. D.J. Morrissey *et al.*, *Nucl. Inst. and Meth.* **B204** (2003) 90.
8. D. Bazin *et al.*, *Nucl. Inst. and Meth.* **A482** (2002) 307.
9. R. Pfaff, PhD thesis Michigan State University (1997)
10. S.M. Lukyanov *et al.*, *J. Phys. G* **28** (2002) L41.
11. M. Notani *et al.*, *Phys. Lett. B* **542** (2002) 49.
12. K. Sümmerner and B. Blank, *Phys. Rev. C* **61** (2000) 034607
13. L. Tassan-Got and C. Stépan, *Nucl. Phys.* **A524** (1991) 121.
14. R. Charity *et al.*, *Nucl. Phys.* **A483** (1988) 391.